

Microbiome compositional analysis with logistic-tree normal models

Zhuoqun Wang
Duke University
Durham, NC 27708

Jialiang Mao
LinkedIn Corporation
Sunnyvale, CA 94085

Li Ma*
Duke University
Durham, NC 27708

September 3, 2021

Abstract

Modern microbiome compositional data are often high-dimensional and exhibit complex dependency among the microbial taxa. However, existing approaches to analyzing microbiome compositional data either do not adequately account for the complex dependency or lack scalability to high-dimensionality, which presents challenges in appropriately incorporating the “random effects” in microbiome compositions in the resulting statistical analysis. We introduce a generative model, called the “logistic-tree normal” (LTN) model, that addresses this need. The LTN marries two popular classes of models—the log-ratio normal (LN) and the Dirichlet-tree (DT)—and inherits the key benefits of each. LN models are flexible in characterizing covariance structure among taxa but lacks scalability to higher dimensions; DT avoids this issue through a tree-based binomial decomposition but at the same time it incurs restrictive covariance among the taxa. The LTN model incorporates the tree-based decomposition as the DT does, but it jointly models the corresponding binomial probabilities using a (multivariate) logistic-normal distribution as in LN models. It therefore allows rich covariance structures as the LN, along with computational efficiency realized through a Pólya-Gamma augmentation on the binomial models associated with the tree nodes. Accordingly, Bayesian inference on the LTN model can readily proceed by Gibbs sampling. The LTN also allows common techniques for effective inference on high-dimensional data—such as those based on sparsity and low-rank assumptions in the covariance structure—to be readily incorporated. Depending on the goal of the analysis, the LTN model can be used either as a standalone model or embedded into more sophisticated hierarchical models. We demonstrate its use in (i) estimating taxa covariance and in (ii) mixed-effects modeling. Finally, we carry out an extensive case study using an LTN-based mixed-effects model to analyze a longitudinal dataset from the T1D cohort of the DIABIMMUNE project.

*Email: li.ma@duke.edu.

1 Introduction

The human microbiome is the collection of genetic information from all microbes residing on or within the human body. The development of high-throughput sequencing technologies has enabled profiling the microbiome in a cost-efficient way through either shotgun metagenomic sequencing or amplicon sequencing on target genes (e.g., the 16S rRNA gene). Various bioinformatic preprocessing pipelines such as MetaPhlAN (Beghini et al., 2021) and DADA2 (Callahan et al., 2016) have been developed to “count” the microbes in each sample and report the results in terms of amplicon sequence variant (ASV) or operational taxonomic unit (OTU) abundance. The resulting datasets are compositional in nature as the total counts of the identified microbes in each sample are determined by the sequencing depth of the study and shall only be interpreted proportionally. Both OTU and ASV can serve as the unit for the downstream analysis of microbial compositions, so for simplicity, we shall use the more classic “OTU” to refer to either of them. Along with the OTU counts, a typical microbiome dataset also contains a summary of the evolutionary relationship of OTUs in the study in the form of a phylogenetic tree, and covariate information on the participant hosts that are usually collected by medical monitoring or questionnaires.

A central task in microbiome studies is to understand the relationship between microbiome compositions with environmental factors such as the dietary habits or the disease status of the hosts. Since individual microbiome samples are noisy and are prone to be polluted by sequencing errors, a popular scientific practice toward this goal is to compare microbiome compositions across groups of samples defined by the factor of interest. For example, a core research question in the DIABIMMUNE study (Kostic et al., 2015) is to understand the association between infant gut microbiome with the type 1 diabetes (T1D) status. To this end, previous studies compared microbiome compositions of case samples with healthy controls and have suggested that the gut microbiome of those T1D cases have significantly lower alpha diversity compared to the controls (Kostic et al., 2015).

Traditionally, such cross-groups comparisons are achieved through either ad-hoc comparisons on lower-dimensional summaries of the microbiomes or distance-based analysis tools like PERMANOVA (McArdle and Anderson, 2001). Alternatively, a more recent thread of works start with a generative model on the microbiome compositions to better account for dependencies among OTUs (Grantham et al., 2017; Tang et al., 2018; Mao et al., 2020; Ren et al., 2020). Cross-group differences are captured by specific parameters in the model. The key to this approach is a flexible generative model on microbiome compositions that account for the features of microbiome count data such as compositionality, high dimensionality, and complex covariance among taxa, which together pose analytical and computational challenges to microbiome data modeling. In addition, it is crucial to adjust for potential confounders and account for the study design in the generative model to properly control for false discoveries.

A common approach to accounting for the compositionality and the count nature of microbiome data is to adopt a multinomial sampling model for the sequencing read counts. Under this strategy, two popular classes of statistical models for the corresponding multinomial probability vector (i.e., the relative abundances of the OTUs) are log-ratio normal (LN) models (Aitchison, 1982) and the more recent Dirichlet-tree multinomial (DTM) model (Dennis III, 1991). The LN model can capture rich covariance structure among the OTUs;

however, inference under such models is computationally challenging when the number of OTUs is large (> 50) due to lack of conjugacy to the multinomial likelihood. The Dirichlet model is another popular model for low-dimensional compositional data. It is conjugate to the multinomial sampling model but its induced covariance structure is characterized by a single scalar parameter, and thus is way too restrictive for microbiome abundances. The DTM is a generalization of the Dirichlet model, designed to lessen this limitation. The DTM preserves the conjugacy by decomposing the multinomial likelihood into a collection of binomials along the phylogenetic tree and modeling the binomial probabilities by beta distributions. With such a decomposition, DTM is conjugate and thus computationally efficient, but the covariance structure, though more relaxed than that of the Dirichlet, is still quite restrictive as it still only uses K parameters to characterize a $K \times K$ covariance structure.

Motivated by these two models, we propose a new generative model called “logistic-tree normal” (LTN) that combines the key features of DTM and LN models to inherit their respective desired properties. LTN utilizes the tree-based decomposition of multinomial model as DTM does but jointly model the binomial probabilities using a multivariate LN distribution with a general covariance structure. By utilizing the tree-based binomial decomposition of the multinomial, LTN restores the full conjugacy with the assistance of Pólya-Gamma data augmentation (Polson et al., 2013), allowing Gibbs sampling for inference and thereby avoiding the computational difficulty incurred by the classic LN models.

The fully probabilistic, generative nature of the LTN model allows it to be used either as a standalone model or embedded into more sophisticated hierarchical models. Moreover, the multivariate Gaussian aspect of the model allows common assumptions for effective inference on high-dimensional data, such as those based on sparsity and low-rank assumptions in the covariance structure, to be readily incorporated while maintaining the computational ease. In this paper, we adopt LTN in a mixed-effects modeling setting to re-analyze the T1D cohort of the DIABIMMUNE study. Like previous analyses, we compare groups of microbiome samples defined by the T1D status as well as multiple diet factors. In the comparison, we adjust for covariates such as age, gender, nationality and dietary records of the participant infants through fixed effects and account for the longitudinal design with random effects. Our analysis confirms previous findings that the introduction of various types of food and the cessation of breastfeeding can drastically change the gut microbiome profile of the infants (Kostic et al., 2015).

In contrast to prior analyses of this study, under the more refined mixed-effects model we find that the microbiome compositions of clinically-labelled T1D patients are not significantly different from those of the healthy controls. Instead, the event of seroconversion marks a “change-point” in the microbiome compositions—it is the samples collected after seroconversion that differ from the others in a statistically significant manner—with the key differences related to the relative abundance of the *Bacteroides* genus and the *Erysipelotrichaceae* family. This implies that abrupt changes in the microbiome composition could potentially be serving as a diagnostic tool for timely detection of seroconversion.

The rest of the paper is organized as follows. Section 2 introduces the LTN model and describes two methodological applications of the model — (1) covariance estimation and (2) mixed-effects modeling. In Section 3, several numerical experiments are carried out to evaluate the performance of our method. In Section 4, we present our analysis on the DIABIMMUNE dataset. Section 5 concludes.

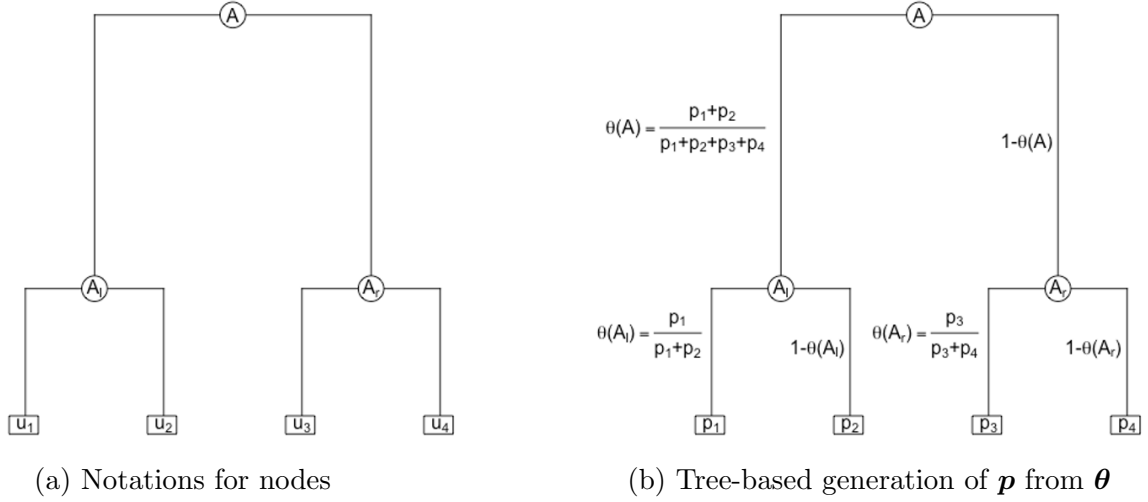


Figure 1: An example of a phylogenetic tree over four OTUs

2 Method

2.1 Logistic-tree normal model for OTU counts

In this section we will briefly review the LN and the DTM models for microbiome compositional data, and then introduce the logistic-tree normal (LTN) model as a combination of these two approaches.

Suppose there are n samples and a total of K OTUs, denoted by u_1, u_2, \dots, u_K . The OTU table is an $n \times K$ matrix, whose i th row represents the OTU counts in sample i and the (i, j) -th element represents the count of OTU j in that sample. Let $\mathcal{T} = \mathcal{T}(\mathcal{I}, \mathcal{U}; \mathcal{E})$ be a rooted full binary phylogenetic tree over the K OTUs, where $\mathcal{I}, \mathcal{U}, \mathcal{E}$ denote the set of interior nodes, leaves, and edges respectively. Formally, we can represent each node A in the phylogenetic tree by the set of its descendent OTUs. Specifically, for a leaf node $A \in \mathcal{U}$, which by definition contains only a single OTU u , we let $A = \{u\}$. Then the interior nodes can be defined iteratively from leaf to root. That is, for $A \in \mathcal{I}$ with two children nodes A_l and A_r , we simply have $A = A_l \cup A_r$. Figure 1a shows an example of a node A containing four OTUs, $\{u_1, u_2, u_3, u_4\}$.

Suppose $\mathbf{X} = (X_1, \dots, X_K)'$ is the OTU counts for a sample, and $N = \sum_{j=1}^K X_j$ is the total number of OTU counts. A natural sampling model for the OTU counts given the total count N is the multinomial model

$$\mathbf{X} \mid N, \mathbf{p} \sim \text{Multinomial}(N, \mathbf{p}), \quad (1)$$

where $\mathbf{p} = (p_1, \dots, p_K)'$ is the underlying OTU (relative) abundance vector, which lies in a $(K - 1)$ -simplex. That is, $\mathbf{p} \in \mathcal{S}_K = \{(p_1, \dots, p_K)' : p_j \geq 0, j = 1, \dots, K, \sum_{j=1}^K p_j = 1\}$. The simplicial constraint on relative abundances can present modeling inconveniences, and a traditional strategy is to apply a so-called log-ratio transformation to map the relative abundance vector into an Euclidean space (Aitchison, 1982).

Three most popular choices of the log-ratio transform are the additive log-ratio (*alr*),

centered log-ratio (*clr*) (Aitchison, 1982) and isometric log-ratio (*ilr*) (Egozcue et al., 2003; Egozcue and Pawłowsky-Glahn, 2016; Silverman et al., 2017), all of which have been applied to microbiome compositional data in the literature. For a composition \mathbf{p} , the *alr* and *clr* transform are defined as follows:

$$clr(\mathbf{p}) = \{\log(p_j/g(\mathbf{p})) : j = 1, \dots, K\},$$

$$alr(\mathbf{p}) = \{\log(p_j/p_K) : j = 1, \dots, d\},$$

where $d = K - 1$ and $g(\mathbf{p})$ is the geometric mean of \mathbf{p} . The *ilr* transform, on the other hand, uses a binary partition tree structure to define the log-ratios, and it turns \mathbf{p} into “balances” associated with the interior nodes of the tree. The balance $\eta(A)$ associated with an interior node A of the tree is defined as

$$\eta(A) = \sqrt{\frac{|A_l||A_r|}{|A_l| + |A_r|}} \log \frac{g(\mathbf{p}(A_l))}{g(\mathbf{p}(A_r))},$$

where $|A_l|$ and $|A_r|$ are the number of OTUs in the left and right subtree of node A respectively, $g(\mathbf{p}(A_l))$ and $g(\mathbf{p}(A_r))$ are the corresponding geometric means of the probability compositions of leaves in the left and right subtrees of node A . While in many applications finding a suitable binary tree for the *ilr* might not be easy, in the microbiome context, the phylogenetic tree is a natural and effective choice (Silverman et al., 2017).

The log-ratio normal (LN) model posits that the log-ratios are multivariate Gaussian. These models have been successfully used in characterizing microbial dynamics (Äijö et al., 2017; Silverman et al., 2018) and linking covariates with microbiome compositions (Xia et al., 2013; Grantham et al., 2017). However, inference using the LN models based on the popular log-ratio transforms can incur prohibitive computational challenges when the number of OTUs grow due to the lack of conjugacy between the multinomial likelihood and multivariate normal.

In contrast, another classical approach to modeling the compositional vector \mathbf{p} that is computationally easier at a (great) cost of flexibility is the Dirichlet model (La Rosa et al., 2012). This model affords only a single scalar parameter to characterize the covariance structure among the OTUs, essentially assuming that all OTUs are independent of each other modulo the artificial dependence caused by the compositional constraint $\sum_j p_j = 1$. This is clearly too restrictive for high-dimensional compositional data such as microbiome compositions.

The Dirichlet-tree multinomial model (DTM) (Dennis III, 1991) has been introduced to alleviate this limitation of the Dirichlet while maintaining computational tractability. Given a dyadic tree \mathcal{T} over the OTUs, e.g., the phylogenetic tree, the DTM utilizes the fact that multinomial sampling is equivalent to sequential binomial sampling down a binary partition. Specifically, the multinomial sampling model in Eq. (1) is equivalent to

$$y(A_l) | y(A), \theta(A) \sim \text{Binomial}(y(A), \theta(A)) \quad \text{for all } A \in \mathcal{I},$$

where

$$y(A) = \sum_{j:u_j \in A} X_j \quad \text{and} \quad \theta(A) = \frac{\sum_{j:u_j \in A_l} p_j}{\sum_{j:u_j \in A} p_j}.$$

See Figure 1b for an illustration.

Under this perspective, the relative abundance vector is now represented using the collection of binomial “branching” probabilities $\theta(A)$ ’s for all $A \in \mathcal{I}$. The DTM model adopts a beta model for each $\theta(A)$ to attain conjugacy with respect to the binomial likelihood. That is,

$$\theta(A) \stackrel{\text{ind}}{\sim} \text{Beta}(\mu(A)\nu(A), (1 - \mu(A))\nu(A)) \quad \text{for } A \in \mathcal{I},$$

where $\mu(A)$ specifies the mean of the branching probabilities and $\nu(A)$ the variance. While it may appear similar to the *ilr*-based LN approach, which also uses the phylogenetic tree in transforming the abundance vector, we note that very importantly the factorization under the DTM is not only providing a transform of \mathbf{p} in terms of the $\theta(A)$ ’s, but is decomposing the *sampling model* (i.e., the multinomial likelihood), which is key to its computational tractability through the beta-binomial conjugacy.

While the DTM model is more flexible than the Dirichlet model, it is far from competitive to the LN model in characterizing the covariance among OTUs. To see this, note that the parameters $\nu(A)$ ’s are the only ones that characterize the covariance across the K OTUs. In fact, the DTM model still assumes independence among the $\theta(A)$ ’s and so there are a total of only d scalar parameters, which along with the underlying phylogenetic tree characterize the covariance among the K OTUs. In contrast, the LN models allow a full $d \times d$ covariance matrix, albeit at a cost of computational tractability.

Motivated by the LN and the DTM, we introduce a hybrid model that combines the tree-based factorization of the multinomial sampling model under the DTM *with* the log-ratio transform under the LN, thereby achieving both the flexibility *and* the computational tractability. Specifically, we adopt a log-ratio transform (i.e., a logistic transform) on the binomial branching probability $\theta(A)$ on each interior node A . That is, we propose to model the log-odds on the interior nodes

$$\psi(A) = \log \frac{\theta(A)}{1 - \theta(A)} \quad \text{for all } A \in \mathcal{I}$$

jointly as multivariate Gaussian.

More formally, for a compositional probability vector $\mathbf{p} = (p_1, p_2, \dots, p_K) \in \mathcal{S}_K$, we define the *tree-based log-ratio* (*tlr*) transform as $\text{tlr}(\mathbf{p}) = \boldsymbol{\psi} = \{\psi(A) : A \in \mathcal{I}\}$, where $\psi(A) = \log \frac{\theta(A)}{1 - \theta(A)}$. Like other log-ratio transforms, *tlr* maps a compositional vector \mathbf{p} to a vector of d log-odds $\psi(A)$. Finally, modeling the *tlr*(\mathbf{p}) as $\text{MVN}(\boldsymbol{\mu}, \boldsymbol{\Sigma})$, we have the full formulation of a *logistic-tree normal* (LTN) model:

$$\begin{aligned} y(A_l) | y(A), \theta(A) &\stackrel{\text{ind}}{\sim} \text{Binomial}(y(A), \theta(A)) \quad \text{for } A \in \mathcal{I}, \\ \psi(A) &= \log \frac{\theta(A)}{1 - \theta(A)} \quad \text{for } A \in \mathcal{I}, \\ \boldsymbol{\psi} &\sim \text{MVN}(\boldsymbol{\mu}, \boldsymbol{\Sigma}). \end{aligned} \tag{2}$$

A graphical model representation of LTN for a dataset with n exchangeable samples is shown in Figure 2a.

At first glance, while the LTN affords flexible mean and covariance structures, it suffers from the same lack of conjugacy as existing LN models based on log-ratio transforms such as *alr*, *clr* and *ilr*. Fortunately, the binomial decomposition of the likelihood under the LTN allows a data-augmentation technique called Pólya-Gamma (PG) augmentation (Polson et al., 2013) to restore the conjugacy.

Following Polson et al. (2013), we can write the binomial likelihood for a sample at an interior node A as

$$p(y(A_l)|y(A), \psi(A)) \propto \frac{(e^{\psi(A)})^{y(A_l)}}{(1 + e^{\psi(A)})^{y(A)}} = 2^{-y(A)} e^{\kappa(A)\psi(A)} \int_0^\infty e^{-w\psi(A)^2/2} f(w) dw,$$

where $\kappa(A) = y(A_l) - y(A)/2$ and

$$f(w) = \frac{2^{y(A)-1}}{\Gamma(y(A))} \sum_{n=0}^{\infty} (-1)^n \frac{\Gamma(n + y(A))}{\Gamma(n + 1)} \frac{(2n + y(A))}{\sqrt{2\pi w^3}} e^{-\frac{(2n+y(A))^2}{8w}}$$

is the probability density function of $\text{PG}(y(A), 0)$ distribution. We can accordingly introduce an auxiliary variable $w(A)$ that is independent of $y(A_l)$ given $y(A)$ and $\psi(A)$, with

$$p(w(A)|y(A), \psi(A)) \propto e^{-w(A)\psi(A)^2/2} f(w(A)).$$

In other words, we add the auxiliary variable $w(A)$ into the LTN model in Eq. (2) with

$$w(A)|y(A), \psi(A) \sim \text{PG}(y(A), \psi(A)).$$

The joint conditional distribution for $w(A)$ and $y(A_l)$ given $y(A)$ and $\psi(A)$ is then

$$p(w(A), y(A_l)|y(A), \psi(A)) \propto 2^{-y(A)} e^{\kappa(A)\psi(A) - w(A)\psi(A)^2/2} f(w(A)),$$

which is a log-quadratic function of $\psi(A)$, and thus is conjugate to the multivariate Gaussian likelihood of $\boldsymbol{\psi} = \{\psi(A) : A \in \mathcal{I}\}$. A graphical model representation of LTN with PG augmentation for a dataset of n exchangeable samples is shown in Figure 2b.

2.2 Methodological applications

Next we demonstrate the broad applicability of LTN in different contexts either as a standalone generative model or as a component in a larger model through two examples: (i) learning the covariance structure among taxa by a sparse (logistic) Gaussian graph; and (ii) building a mixed-effects model on the compositional counts for longitudinal studies. In this section, we shall focus on describing the models and inference algorithms, and will provide numerical examples later in Section 3.

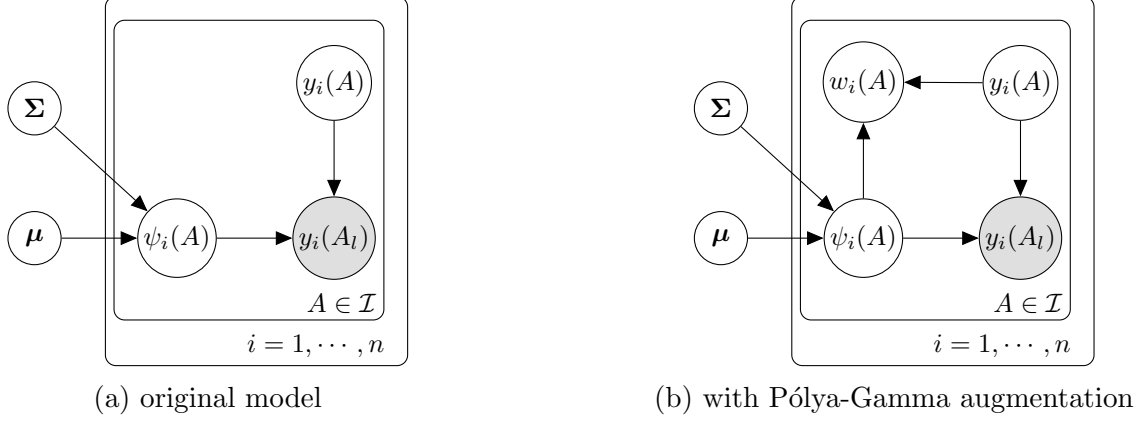


Figure 2: A graphical model representation of LTN for n exchangeable samples

2.2.1 Covariance estimation through a sparse logistic Gaussian graph

A common task in microbiome analysis is to learn the covariance structure or network of the microbial taxa, which can shed light on the underlying biological interplay. Equipped with the LTN model, one can resort to the rich armory of covariance/graphical models in the multivariate analysis literature to accomplish this goal. Here we adopt a graphical modeling approach by assuming a sparse Gaussian graph, i.e., one with a sparse inverse covariance matrix, on the tree-based log-odds $\psi_i(A)$, and carrying out inference in a Bayesian fashion through adopting a popular prior for sparse Gaussian graphs called the graphical Lasso prior (Wang, 2012) on the inverse covariance.

Specifically, the graphical Lasso prior on the precision matrix $\mathbf{\Omega} = \mathbf{\Sigma}^{-1}$ takes the form

$$p(\mathbf{\Omega}|\lambda) = C^{-1} \prod_{j < j'} \{\text{DE}(\omega_{jj'}|\lambda)\} \prod_{j=1}^d \{\text{EXP}(\omega_{jj}|\lambda/2)\} 1_{\mathbf{\Omega} \in M^+}, \quad (3)$$

where $\text{DE}(x|\lambda) = \lambda/2\text{EXP}(-\lambda|x|)$ is the double exponential density function, $\text{EXP}(x|\lambda) = \lambda \exp(-\lambda x) 1_{x>0}$ is the exponential density function, M^+ is the space of positive definite matrices, and C is the normalizing constant that does not involve $\mathbf{\Omega}$ or λ . We denote this distribution with $\text{glasso}(\lambda)$. Finally, we adopt a multivariate Gaussian prior on μ .

Putting all pieces together, we obtain the following model for a dataset of n exchangeable samples:

- sampling model on \mathbf{y}_i for $i = 1, \dots, n$:

$$y_i(A_l) | \psi_i(A), y_i(A) \stackrel{\text{ind}}{\sim} \text{Binomial} \left(y_i(A), \frac{e^{\psi_i(A)}}{e^{\psi_i(A)} + 1} \right) \quad \text{for all } A \in \mathcal{I},$$

$$\psi_i | \mu, \mathbf{\Omega} \stackrel{\text{iid}}{\sim} \text{MVN}(\mu, \mathbf{\Omega}^{-1}),$$

- prior on μ :

$$\mu \sim \text{MVN}(\mathbf{0}, \mathbf{\Lambda}),$$

- prior on $\mathbf{\Omega}$:

$$\mathbf{\Omega}|\lambda \sim \text{glasso}(\lambda),$$

where $\lambda, \mathbf{\Lambda}$ are hyperparameters and we set $\mathbf{\Lambda} = 5\mathbf{I}$ in the numerical examples. The shrinkage parameter λ can either take a fixed value or be further modeled with a Gamma hyperprior.

After introducing the PG auxiliary variables

$$w_i(A)|y_i(A), \psi_i(A) \stackrel{\text{ind}}{\sim} \text{PG}(y_i(A), \psi_i(A)) \quad \text{for } A \in \mathcal{I} \text{ and } i = 1, \dots, n$$

all terms in this model except $\mathbf{\Omega}$ are conditionally conjugate. To effectively sample $\mathbf{\Omega}$, we adopt a further data augmentation scheme proposed in Wang (2012), which makes all full conditionals available in closed form allowing (blocked) Gibbs sampling. Specifically, because the double exponential distribution on the off-diagonal terms of $\mathbf{\Omega}$ is a scale mixture of normals, by introducing latent scale parameters $\boldsymbol{\tau} = \{\tau_{jj'} : 1 \leq j < j' \leq d\}$, the data-augmented target distribution can be expressed as follows:

$$p(\mathbf{\Omega}, \boldsymbol{\tau}|\boldsymbol{\mu}, \boldsymbol{\psi}, \lambda) \propto |\mathbf{\Omega}|^{n/2} \exp \left\{ -\text{tr} \left(\frac{1}{2} \mathbf{S} \mathbf{\Omega} \right) \prod_{j < j'} \left\{ \tau_{jj'}^{-1/2} \exp \left(-\frac{\omega_{jj'}^2}{2\tau_{jj'}} - \frac{\lambda^2}{2} \tau_{jj'} \right) \right\} \right\} \times \prod_{j=1}^d \left\{ \exp \left(-\frac{\lambda}{2} \omega_{jj} \right) \right\} 1_{\mathbf{\Omega} \in M^+}, \quad (4)$$

where $\mathbf{S} = \sum_{i=1}^n (\boldsymbol{\psi}_i - \boldsymbol{\mu})(\boldsymbol{\psi}_i - \boldsymbol{\mu})^T$, and the marginal distribution of $\mathbf{\Omega}$ is the graphical Lasso distribution with parameter λ .

We summarize the blocked Gibbs sampler with a $\text{Gamma}(r, s)$ hyperprior on λ in Algorithm 1. In the sampler, for any square matrix $\mathbf{A} = (A_{jj'})$, $\mathbf{A}_{-j, -j}$ denotes the submatrix of \mathbf{A} formed by removing the j th row and j th column, and $\mathbf{A}_{j, -j}$ the row vector formed by removing A_{jj} from the j th row of \mathbf{A} . For given values $\lambda^{(t)}, \mathbf{\Omega}^{(t)}, \boldsymbol{\tau}^{(t)}, \boldsymbol{\mu}^{(t)}$, let $\boldsymbol{\Upsilon}^{(t)} = (\boldsymbol{\tau}_{jj'}^{(t)})$ be a $d \times d$ symmetric matrix with zeros in the diagonal entries and $\boldsymbol{\tau}^{(t)}$ in the upper diagonal entries, and define $\mathbf{C}_j^{(t)} = ((S_{jj}^{(t)} + \lambda^{(t)})(\mathbf{\Omega}_{-j, -j}^{(t)})^{-1} + \text{diag}(\boldsymbol{\Upsilon}_{j, -j}^{(t)}))^{-1}$.

The blocked Gibbs sampler allows drawing from the joint posterior of all parameters in the model. In particular, it generates posterior samples for the log-odds parameters $\psi_i(A)$. If the practitioner wants to investigate the posterior of the original relative abundances or that under a different transform such as *alr*, *clr* and *ilr*, one can easily apply the inverse *tlr* to attain samples for the original relative abundance, which can be further transformed as desired.

2.2.2 Mixed-effects modeling for microbiome compositions

Next we consider a methodological application of the LTN model in mixed-effects modeling. Mixed-effects models are arguably the most useful statistical device for incorporating study designs into modeling microbiome compositions. Common design features such as covariates, batch effects, multiple time points, and replicates can all be readily incorporated.

For demonstration, consider a common study design where a dataset involves n samples that can be categorized into two contrasting groups (e.g., case vs control, treatment vs

Algorithm 1 Blocked Gibbs sampler for LTN with $\text{glasso}(\lambda)$ prior on precision matrix

```

Initialize  $\mathbf{w}^{(0)}, \boldsymbol{\psi}^{(0)}, \boldsymbol{\Omega}^{(0)}, \boldsymbol{\tau}^{(0)}, \boldsymbol{\mu}^{(0)}$ .
for  $t = 1, \dots, T$  do
  1. Update  $\mathbf{w}$ :
  for  $i = 1, \dots, n$  do
    for  $A \in \mathcal{I}$  do
      Draw  $w_i^{(t)}(A) \sim \text{PG}(y_i^{(t-1)}(A), \psi_i^{(t-1)}(A))$ 
    end for
  end for
  2. Update  $\boldsymbol{\psi}$ :
  for  $i = 1, \dots, n$  do
    Draw  $\boldsymbol{\psi}_i^{(t)} \sim \text{MVN}\left((\boldsymbol{\Omega}^{(t-1)} + \text{diag}(\mathbf{w}_i^{(t-1)}))^{-1}(\boldsymbol{\Omega}^{(t-1)}\boldsymbol{\mu}^{(t-1)} + \boldsymbol{\kappa}_i), (\boldsymbol{\Omega}^{(t-1)} + \text{diag}(\mathbf{w}_i^{(t-1)}))^{-1}\right)$ 
  end for
  3. Update  $\boldsymbol{\mu}$ :
  Draw  $\boldsymbol{\mu}^{(t)} \sim \text{MVN}((\boldsymbol{\Lambda}^{-1} + n\boldsymbol{\Omega}^{(t-1)})^{-1}\boldsymbol{\Omega}^{(t-1)}\sum_{i=1}^n \boldsymbol{\psi}_i^{(t)}, (\boldsymbol{\Lambda}^{-1} + n\boldsymbol{\Omega}^{(t-1)})^{-1})$ 
  4. Update  $\boldsymbol{\Omega}$  and  $\boldsymbol{\tau}$ 
  for  $j = 1, \dots, d$  do
    Draw  $\gamma \sim \text{Gamma}(n/2 + 1, (S_{jj}^{(t-1)} + \lambda^{(t-1)})/2)$ 
    Draw  $\boldsymbol{\beta} \sim \text{MVN}(-\mathbf{C}_j^{(t-1)}\mathbf{S}_{j,-j}^{(t-1)}, \mathbf{C}_j^{(t-1)})$ 
    Update  $\boldsymbol{\Omega}_{j,-j}^{(t)} = \boldsymbol{\beta}, \boldsymbol{\Omega}_{-j,j}^{(t)} = \boldsymbol{\beta}^T, \Omega_{jj}^{(t)} = \gamma + \boldsymbol{\beta}^T(\boldsymbol{\Omega}_{-j,-j}^{(t)})^{-1}\boldsymbol{\beta}$ 
  end for
  for  $1 \leq j < j' \leq d$  do
    Draw  $u_{jj'} \sim \text{Inv-Gaussian}(\sqrt{(\lambda^{(t-1)})^2/(\Omega_{jj'}^{(t)})^2}, (\lambda^{(t-1)})^2)$ 
    Update  $\tau_{jj'}^{(t)} = 1/u_{jj'}$ 
  end for
  5. Update  $\lambda$ :
  Draw  $\lambda^{(t)} \sim \text{Gamma}\left(r + p(p+1)/2, s + \frac{1}{2}\sum_{j=1}^d\sum_{j'=1}^d |\Omega_{jj'}^{(t)}|\right)$ 
end for

```

placebo, etc.), and the practitioner is interested in testing whether there is cross-group difference in microbiome compositions. For each microbiome composition sample i , let $s_i \in \{0, 1\}$ be the group indicator and \mathbf{z}_i a q -vector of covariates.

We consider random effects that involve measured subgrouping structure (e.g., individuals). Specifically, we assume that there is a random effect for each sample associated with an observed grouping $g_i \in \{1, \dots, G\}$. For example, in longitudinal studies, g_i can represent the individual from which the i th sample is collected. We associate the covariates and random effects with the microbiome composition through the following linear model:

$$\boldsymbol{\psi}_i = \boldsymbol{\alpha}s_i + \boldsymbol{\beta}^T\mathbf{z}_i + \boldsymbol{\gamma}_{g_i} + \boldsymbol{\epsilon}_i,$$

where $\boldsymbol{\alpha}$ represents the potential cross-group differences, $\boldsymbol{\beta}$ is a $q \times d$ matrix of unknown fixed effect coefficients of the covariates, $\boldsymbol{\gamma}_{g_i}$ is the random effect from individual g_i , which we model exchangeably as $\boldsymbol{\gamma}_g \stackrel{\text{iid}}{\sim} \text{MVN}(\mathbf{0}, \boldsymbol{\Sigma})$ for $g = 1, \dots, G$, and $\boldsymbol{\epsilon}_i(A) \stackrel{\text{ind}}{\sim} \text{N}(0, \sigma_\epsilon^2(A))$. We

adopt inverse-Gamma prior on $\sigma_\epsilon^2(A)$.

Under this formulation, testing two-group difference can be accomplished through testing a collection of hypotheses on the interior nodes:

$$H_0 : \alpha(A) = 0 \text{ versus } H_1 : \alpha(A) \neq 0.$$

To perform these local tests, we adopt a Bayesian variable selection strategy and place the following spike-and-slab priors on entries of $\boldsymbol{\alpha}$:

$$\begin{aligned} \alpha(A) | \pi(A), \phi_\alpha &\stackrel{\text{iid}}{\sim} (1 - \pi(A))\delta_0 + \pi(A)(1 - \delta_0)\text{N}(0, 1/\phi_\alpha) & \text{for } A \in \mathcal{I}, \\ \pi(A) &\stackrel{\text{iid}}{\sim} \text{Beta}(m, 1 - m) & \text{for } A \in \mathcal{I}, \\ \phi_\alpha &\sim \text{Gamma}(t, u), \end{aligned}$$

where δ_0 is point mass at 0, and m, t, u are pre-specified hyperparameters. Note that the prior probability of the null hypothesis that there is no cross-group difference is $\Pr(\boldsymbol{\alpha} = \mathbf{0}) = (1 - m)^d$. To achieve a given value c of this probability, we set $m = 1 - c^{1/d}$. We adopt continuous priors on the coefficients of the covariates: $\boldsymbol{\beta} \sim \text{N}_{q \times d}(0, 100n\mathbf{I}_d \otimes (\mathbf{Z}^T \mathbf{Z})^{-1})$.

Existing literature on microbiome mixed-effects modeling have adopted the low-rank assumption on the covariance structure through introducing latent factors (Grantham et al., 2017; Ren et al., 2020). We believe that sparsity assumption can also be very useful in this context. In fact, there is no clear rationale to impose sparsity in covariance estimation but not in random effects modeling, as they are modeling exactly the same type of covariance structure.

The LTN framework allows both low-rankness and sparsity to be readily incorporated using existing techniques in multivariate analysis. For demonstration and to investigate the usefulness of sparsity in this context, in the following example we again impose sparsity by adopting a graphical Lasso prior on the covariance of random effects,

$$\boldsymbol{\Omega} = \boldsymbol{\Sigma}^{-1} | \lambda \sim \text{glasso}(\lambda).$$

Posterior sampling on this model can again be conducted using a blocked Gibbs sampler, where $\boldsymbol{\Omega}$ is updated with a procedure similar to the one in Section 2.2.1. With the PG augmentation, all parts of the model can be drawn from conjugate full conditionals. The details of the sampler are included in Supplementary Materials A.

Based on the posterior samples, we can compute $\Pr(\alpha(A) \neq 0 | \mathbf{Y})$, the *posterior marginal alternative probability* (PMAP) for each $A \in \mathcal{I}$, and $\Pr(\boldsymbol{\alpha} \neq \mathbf{0} | \mathbf{Y})$, the *posterior joint alternative probability* (PJAP). The PJAP can be used as a test statistics for rejecting the null hypothesis that no difference at all exists in any microbial taxa between the two groups, whereas PMAP can be used to investigate what microbial taxa are actually different across groups should PJAP indicates that such a difference exists. Both the PMAPs and PJAP can be directly estimated from the posterior samples of $\boldsymbol{\alpha}$.

3 Numerical examples

In this section, we carry out simulation studies to demonstrate the work of LTN in (i) covariance estimation and (ii) two-group comparison based on a mixed-effects model as described in Section 2.2.2.

3.1 Covariance estimation

3.1.1 Simulation settings

We simulate datasets with $N = 200$ samples and $K = 50$ OTUs, where the OTU counts are generated from both LN and DTM models using the phylogenetic tree from the DIA-BIMMUNE data (Kostic et al., 2015). We note that under the LN settings, the tree-based log-odds $\psi_i(A)$'s are not normally distributed. Under the DTM setting, LTN does not assume the correct distributional form of \mathbf{p}_i either. We purposefully simulate from these models that are different from our adopted model to show that even under such model misspecification, the LTN can recover the true covariance structure in a robust manner. The simulation setup is described as follows:

1. **log-ratio normal (LN).** The OTU counts $\mathbf{X}_1, \dots, \mathbf{X}_{200}$ are generated from the following model:

$$\begin{aligned}\mathbf{X}_i | \mathbf{p}_i &\stackrel{\text{ind}}{\sim} \text{Multinomial}(10^5, \mathbf{p}_i) \\ \mathbf{p}_i &= \text{ilr}^{-1}(\boldsymbol{\eta}_i) \\ \boldsymbol{\eta}_i &\stackrel{\text{iid}}{\sim} \text{MVN}(\mathbf{m}, \boldsymbol{\Omega}_0^{-1})\end{aligned}$$

where ilr^{-1} is the inverse of the ilr transform based on the phylogenetic tree (Silverman et al., 2017). The components of \mathbf{m} are independent samples from $N(0, 16)$.

We adopt three models – Hub, Block and Sparse for $\boldsymbol{\Omega}_0$, which are considered by Cao et al. (2019) as plausible covariance models for microbiome compositions.

Hub: The 50 OTUs are randomly divided into 3 hubs and 47 non-hub points, where $\Pr(\text{hub connected to other OTU}) = 0.7, \Pr(\text{two non-hub OTUs are connected}) = 0.2$. Each non-zero entry is set to 0.3 (with probability 0.5) or -0.3 (with probability 0.5). The diagonal entries are set large enough so that $\boldsymbol{\Omega}_0$ is positive definite.

Block: The OTUs are equally divided into 10 blocks. Each pair of points in the same block are connected with probability 0.5, while each pair between different blocks are connected with probability 0.2. Each non-zero entry is set to 0.3 (with probability 0.5) or -0.3 (with probability 0.5). The diagonal entries are set large enough so that $\boldsymbol{\Omega}_0$ is positive definite.

Sparse: Let

$$\boldsymbol{\Omega}_0 = \begin{pmatrix} \mathbf{A}_1 & \mathbf{0} \\ \mathbf{0} & \mathbf{I}_{p_2} \end{pmatrix},$$

where $\mathbf{A}_1 = \mathbf{B} + \epsilon \mathbf{I}_{p_1}, p_1 = \lfloor 3\sqrt{d} \rfloor, p_2 = d - p_1$, \mathbf{B} is a $p_1 \times p_1$ symmetric matrix whose lower triangular entries are defined as $B_{ij} = U_{ij} 1_{V_{ij} < 0.3}$, where $U_{ij} \stackrel{\text{iid}}{\sim}$

$\text{Unif}([-1, -0.5] \cup [0.5, 1])$, $V_{ij} \stackrel{\text{iid}}{\sim} \text{Unif}([0, 1])$, U_{ij} and V_{ij} are independent, and ϵ is large enough so that \mathbf{A}_1 is positive definite. Under this simulation setting, there is an underlying sparse network of the interior nodes of the phylogenetic tree in each dataset.

2. **DTM.** Under this scenario, the samples $\mathbf{X}_1, \dots, \mathbf{X}_{200}$ are generated from the following DTM model:

$$\begin{aligned}\mathbf{X}_i | \mathbf{p}_i &\stackrel{\text{ind}}{\sim} \text{Multinomial}(10^5, \mathbf{p}_i) \\ \mathbf{p}_i &\stackrel{\text{iid}}{\sim} \text{DT}(\boldsymbol{\theta}, \boldsymbol{\tau}),\end{aligned}$$

where DT is the Dirichlet-tree distribution. We adopt the phylogenetic tree from the subset of the DIABIMMUNE data to be described in Section 3.2.1, and set $\boldsymbol{\theta}$ and $\boldsymbol{\tau}$ to their method of moments estimates based on the same dataset.

3.1.2 Comparison to a state-of-the-art benchmark

To judge the performance of our approach, we use as a benchmark a state-of-the-art approach called COAT recently introduced in Cao et al. (2019), and consider four different loss functions—the Frobenius norm ($\|\cdot\|_F$), L_1 norm ($\|\cdot\|_1$), entry-wise L_∞ norm ($\|\cdot\|_{\max}$) and the spectral norm ($\|\cdot\|_2$) of the difference between the estimated *clr* correlation matrix and the truth. We examine these losses on the *clr* correlation matrix because COAT aims at estimating the *clr* covariance and so this choice is the most appropriate when using COAT as the benchmark.

Table 1: Comparisons of risks of two methods under different simulation settings

	LN-Hub		LN-Block		LN-Sparse		DTM	
	LTN	COAT	LTN	COAT	LTN	COAT	LTN	COAT
Frobenius	18.99	22.28	17.67	18.96	20.39	24.40	5.19	4.93
L_1	28.07	37.48	26.63	34.46	30.90	36.68	6.13	8.38
L_∞	1.25	1.62	1.27	1.55	1.32	1.59	0.67	0.88
Spectral	16.96	16.78	15.46	14.31	16.75	18.64	3.12	3.46

The results are presented in Table 1. Here we set $\lambda = 10$ in LTN. More results under other choices of λ are provided in the Supplementary Material (Table S1 - S4). Under the LN-sparse setting, LTN outperforms COAT under all four losses. Under the other simulation settings, LTN outperforms COAT under most losses. The flexibility of the multivariate normal allows LTN to effectively characterize the cross-sample variability even when the distribution of the relative abundances is misspecified.

3.2 Cross-group comparison based on a mixed-effects model

3.2.1 Simulation settings

Next we demonstrate LTN in mixed-effects modeling. Synthetic datasets are generated based on the 16S sequence data of Type 1 diabetes (T1D) cohort of DIABIMMUNE project

(Kostic et al., 2015), which collects longitudinal microbiome samples from 33 infants from Finland and Estonia. The full dataset contains counts of 2240 OTUs from 777 samples. The main goal of this study is to compare microbiome in infants who have developed T1D or serum autoantibodies (markers predicting the onset of T1D) with healthy controls in the same area. Within the time-frame of the study, 11 out of 33 infants seroconverted to serum autoantibody positivity, and of those 11 infants, four developed T1D. For illustration purpose, we focus on the 50 OTUs with the highest relative abundance and narrow down the samples to healthy infants in Finland. The phylogenetic tree \mathcal{T} of the 50 OTUs is used throughout all simulations.

We simulate data from both the null and the alternative hypotheses, corresponding to the absence and presence of cross-group differences. Datasets under the null are created by randomly dividing the samples into two equal-sized groups. Two different scenarios of the alternative are considered:

1. Cross-group difference exists at a single OTU. In each simulation, we randomly select one of the top 20 OTUs with the highest relative abundance and increase the count of this OTU by 200% in the second group.
2. Cross-group difference exists at multiple OTUs. In each simulation, we randomly select eight OTUs from the top 20 OTUs and increase the count of these OTUs by 50% in the second group.

We fit the mixed-effects model described in Section 2.2.2 to test the existence of differences in microbiome compositions across the two groups. Age at collection is included as a fixed effect, and individuals from which the samples were taken are treated as random effects.

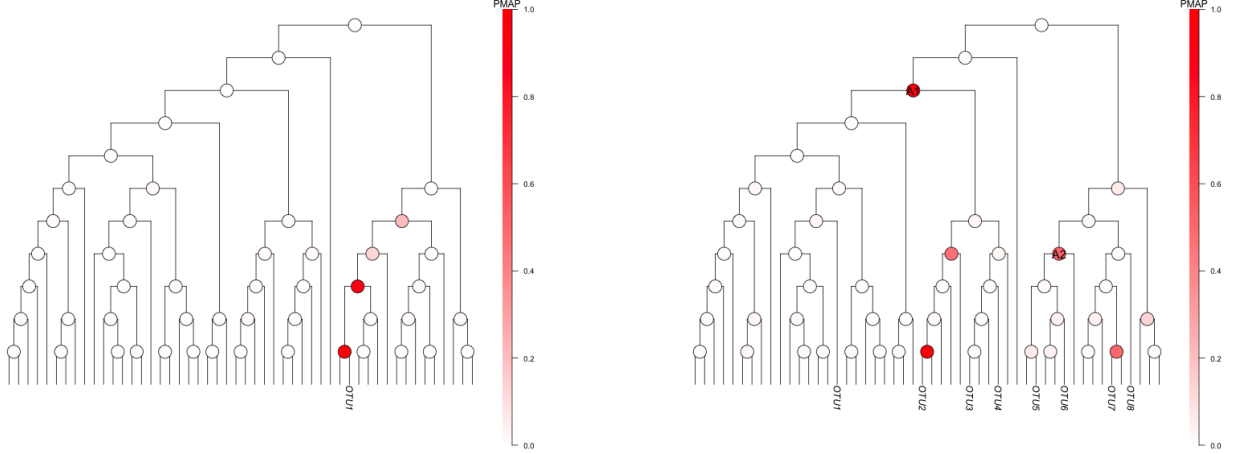
3.2.2 Characterization of cross-group differences through PMAPs

The capability of LTN in characterizing the cross-group differences under the two simulation scenarios can be seen from the PMAP plots from two specific simulation runs. Figure 3a presents the PMAPs from LTN under a specific simulation case in Scenario 1 as an example. LTN correctly identifies the path where the cross-group differences exist, and the decaying pattern of the signal along the path from the parent node of the selected OTU to the root of the tree can be clearly seen. In practice, such a path can be used to narrow the range of cross-group difference down to a certain taxon.

Under Scenario 2, the cross-group difference at each of the selected OTUs are much smaller than that in Scenario 1. However, with the tree-based transform, the weak signals at multiple OTUs are aggregated at their common ancestors. We take a specific round of simulation under this scenario as an illustration. As shown in Figure 3b, the cross-group differences at OTUs 2, 3, and 4 are revealed by the large PMAP at node A_1 , and the cross-group differences at OTUs 5 and 6 are revealed by the large PMAP at node A_2 .

3.2.3 Comparison to a state-of-the-art benchmark

We examine the performance of the proposed mixed-effects model in testing the null that there is no cross-group difference using a state-of-the-art mixed-effects model for microbiome



(a) Scenario 1. The selected OTU is marked as “OTU1”.

(b) Scenario 2. The selected OTUs are marked as “OTU1”, ..., “OTU8”.

Figure 3: PMAPs from LTN under a certain simulation round in each scenario

compositions called DirFactor (Ren et al., 2020) as the benchmark. DirFactor induces a marginal Dirichlet process prior for the OTU compositions and assumes a low-rank covariance structure in the random effects. To parse out how much of the performance difference can be attributed to (1) the LTN model and (2) the sparsity assumption, we include two variants of our LTN approach—one adopting a graph Lasso prior on the precision matrix Ω , and the other forcing the precision matrix to be diagonal.

We present the ROC curves of these two approaches for the two alternative scenarios in Figure 4. Under both scenarios, LTN has higher power than DirFactor at low to moderate false positive rates. Under Scenario 1, the ROC curve of LTN with sparse precision matrix dominates that of the diagonal precision matrix, which reveals the advantage of a more flexible covariance structure among the nodes. Under Scenario 2, the power under the LTN with diagonal precision matrix and sparse precision matrix are similar, and are higher than that under DirFactor. Thus it is likely that the better performance results from adopting LTN distribution on \mathbf{p}_i . Moreover, the impressive performance of LTN under Scenario 2 is likely due to the aggregation of signals at the interior nodes discussed in Section 3.2.2.

The ROC curves under a wider range of λ is provided in the Supplementary Material as a sensitivity analysis (Figure S2). In practice, we recommend using $\lambda \in [1, 10]$ for a moderate level of shrinkage and robust results.

4 Case study: The DIABIMMUNE data

In this section, we apply the mixed-effects model described in Section 2.2.2 to the Type 1 diabetes (T1D) cohort of DIABIMMUNE project to study the relationship of microbiome composition with certain host-level covariates. Previous studies on this dataset have established associations between the microbiome composition with both the T1D status as well as environmental and diet factors. For example, it has been shown that the microbiome of

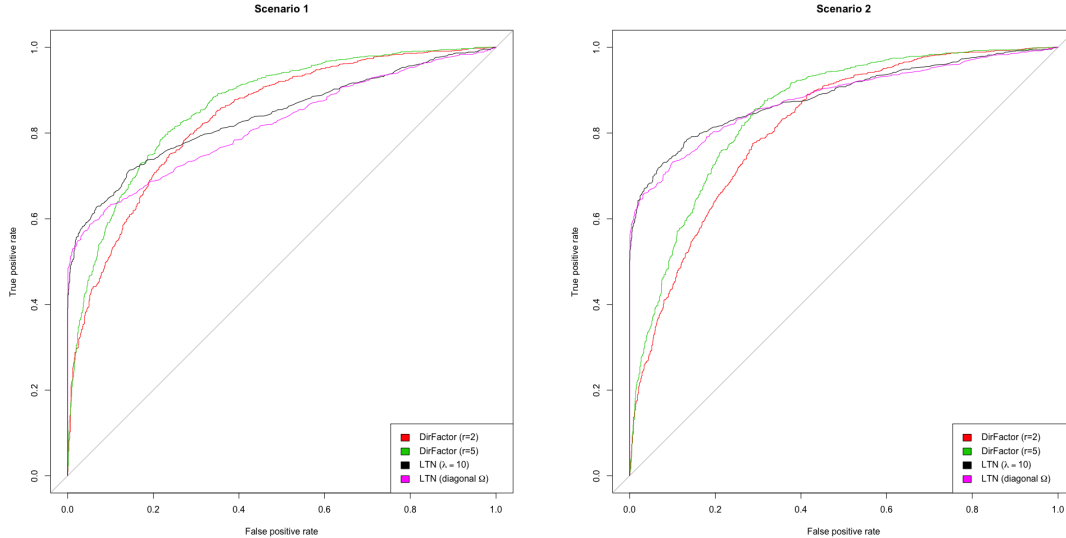


Figure 4: ROC curves under the two simulation scenarios. r is the number of latent factors in DirFactor.

T1D patients tends to have a reduced diversity and increased prevalence of *Bacteroidetes* taxa (Dedrick et al., 2020; Kostic et al., 2015; Brugman et al., 2006). We focus on T1D status and dietary covariates and study the relationship between microbiome composition with each of the factors. Specifically, our analysis takes three steps for each single factor: (1) dichotomize the samples into two groups based on the level or value of the factor; (2) compare the microbiome compositions at the group level; and (3) identify and report the taxa that show such differences.

Our study differs from previous studies from both statistical and scientific perspectives. Statistically, unlike in the MaAsLin method used in Kostic et al. (2015) that fits a generalized linear model on the arcsine square root transformed relative abundance of each OTU independently, we model the OTU counts jointly. By directly accounting for the compositional nature and the dependency structure among OTUs, false discoveries of cross-group differences are controlled in a more coherent way. Scientifically, our analysis identifies the cross-group differences in a standardized manner on the nodes of the phylogenetic tree across different taxonomy levels. In comparison, previous studies first pick a specific level in an ad hoc manner and aggregate OTU counts to that level for the analyses. However, different levels of aggregation can result in inconsistent findings (Mao et al., 2020; Tang et al., 2018). In addition, LTN also provides a natural way to report and visualize such differences in terms of PMAPs along the phylogenetic tree.

Key scientific findings from our analysis are summarized as follows: (i) the microbiome compositions of samples collected from T1D cases and seroconverters are not significantly different from the healthy controls; (ii) the microbiome compositions of samples taken after seroconversion differ from the other samples in terms of the relative abundance within two taxa: the genus *Bacteroides* and the family *Erysipelotrichaceae*, which are different from the taxa associated with T1D identified in Kostic et al. (2015); (iii) introduction of several kinds of food and cessation of breastfeeding can significantly alter the gut microbiome of the

infants; in particular, all of these alternations involve taxa within the order Clostridiales. We present details of our study on different host-level factors in the following sections.

4.1 T1D status

The DIABIMMUNE dataset records the T1D status of the individuals at the end of the study as one of the three levels: control, seroconverted and T1D onset. This status is used to define the case and control groups, where the case group consists of both seroconverted individuals and those who are clinically classified as T1D. For those in the case group, the age at seroconversion is also recorded.

We perform two comparisons regarding the T1D status variable. Firstly, a classic case vs. control comparison is provided to retrospectively determine the association between gut microbiome and T1D. Previous study on the T1D status reveals that after the “seroconversion window” (i.e., the time between the first and third quartiles of age at seroconversion for all seroconverted and T1D subjects), the alpha-diversity of microbial communities in T1D subjects showed a significant flattening, while the alpha diversity in other subjects continue to increase, and such difference can be accounted for by several groups of bacteria (Kostic et al., 2015). Motivated by these findings, we also perform a second comparison between the samples collected after seroconversion and the others to detect potential changes in microbiome compositions after seroconversion.

In each comparison, we include a set of environmental and diet factors that might be associated with the microbiome composition as fixed effects to control false positives. First, we include eight binary dietary variables that indicate whether a specific type of diet was consumed at the time when the sample was collected: *breastfeeding*, *solid food*, *eggs*, *fish*, *soy products*, *rye*, *barley*, and *buckwheat and millet*. Age at collection (log-transformed), gender and nationality of the individuals are also included as fixed effects. In addition, individual random effects are included to account for the between-individual variation.

We note that adjusting for these covariates are crucial for identifying the real cross-group differences. Fig. 5 shows the multidimensional scaling results of the Bray-Curtis dissimilarity between samples, where age at collection increases almost in the same direction of the first axis, and the Finish and Estonian samples are roughly separated along the second axis, especially in the case group. As shown in Fig. 6, the most abundant phylum has larger between-individual and within-individual variability at the very beginning of life, and stabilizes over time. For this reason, we take log transform of age to account for the more rapid changes in microbiome compositions at early age. Interestingly, seroconversion generally happens after the highly variable phase. Most samples collected after one year old are dominated with either Bacteroidetes or Firmicutes. Moreover, it is worth noting that Actinobacteria dominates other taxa in most samples collected from Estonian individuals during the first year, while that’s not the case for Finnish individuals.

We focus on the top 50 OTUs with highest relative abundance and take $\lambda = 10$. The PJAPs of the case/control and pre-/post-seroconversion comparisons are 0.49 and 1.00, respectively. Overall there is no sufficient evidence that the microbiome composition distinguishes the cases and controls; instead, there are significant changes in the relative abundance of certain taxa, though might not be consequences of seroconversion, occur around the time of seroconversion.

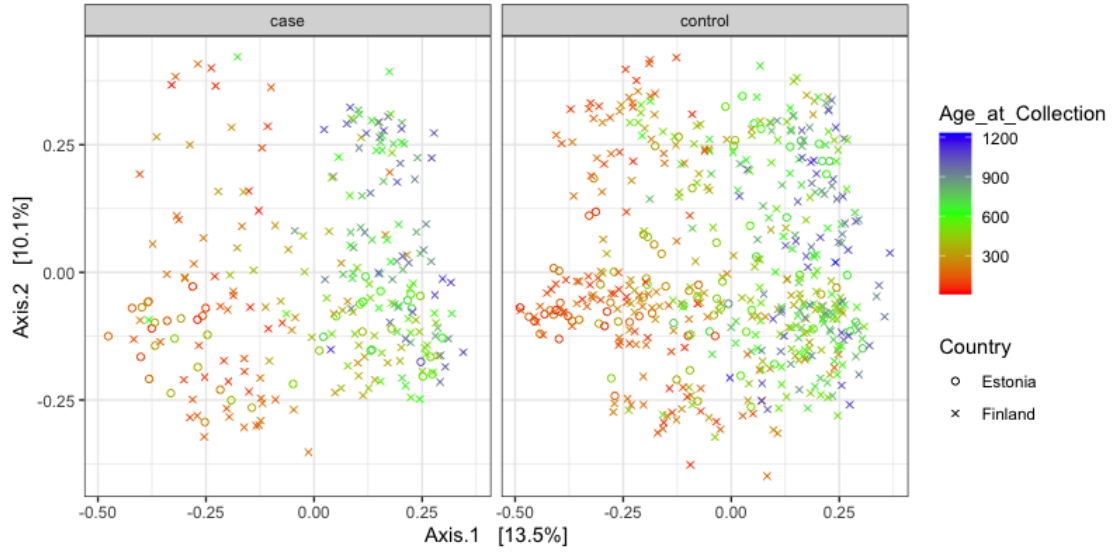


Figure 5: Multidimensional scaling of Bray-Curtis dissimilarity between samples

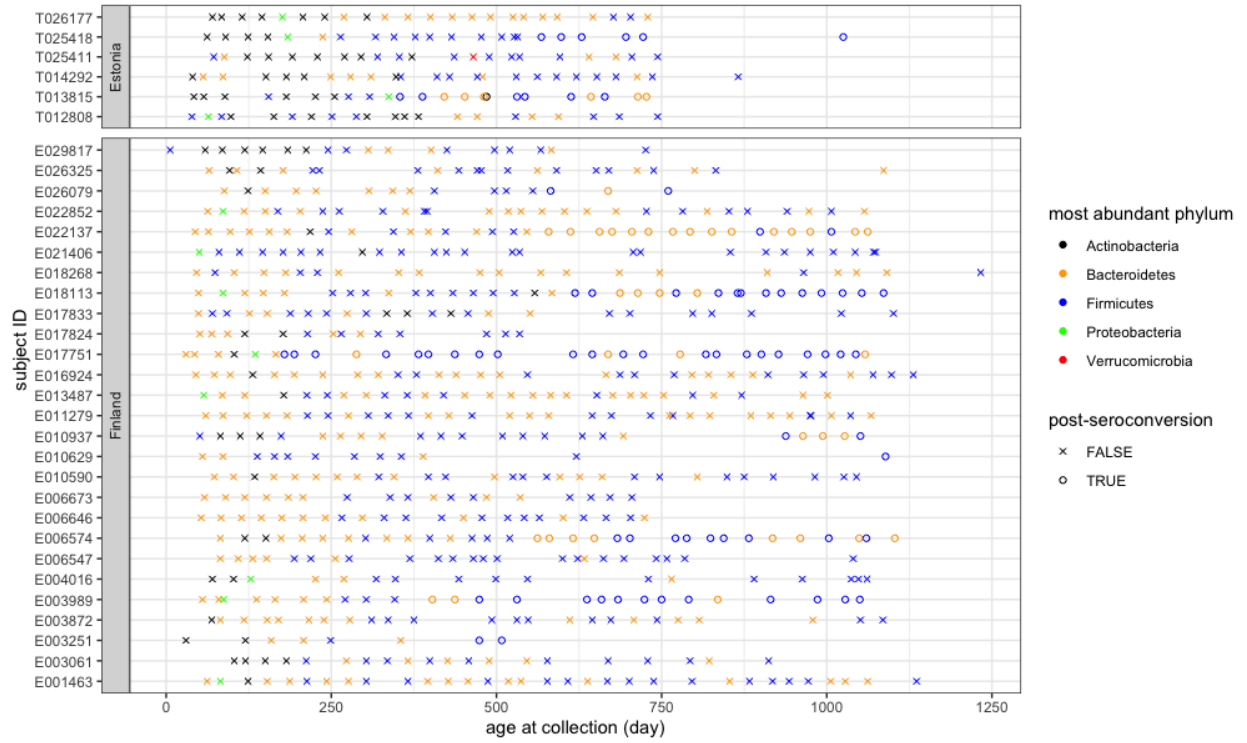


Figure 6: The most abundant phylum in each sample

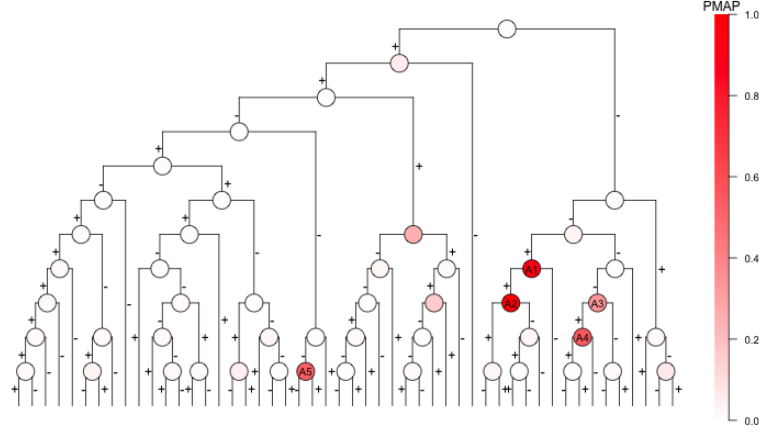


Figure 7: PMAPs of seroconversion. The nodes are colored by PMAP. For each node A , the sign of posterior mean of $\alpha(A)$ is marked with “+”/“−” on left and right branches.

To inspect the patterns of such changes and the associated taxa, we plot the PMAPs in the pre-/post-seroconversion along the phylogenetic tree (Fig. 7). Large PMAPs occur within two taxa: the *Bacteroides* (node A1-A4) and *Erysipelotrichaceae* (node A5). The chain from node A2 to A1 and from A4 to A3 suggests a relatively higher abundance of the left descendant branches of A2 and A4 in the post-seroconversion group. This result resonates with previous findings that *Bacteroides ovatus* (the left child of A4) has a significantly higher relative abundance in T1D cases than in healthy controls at the time of autoimmunity (Giongo et al., 2011), and *Bacteroides* taxa and unclassified *Erysipelotrichaceae* species in general tend to have increased prevalence in T1D cases or islet autoimmunity cases (Davis-Richardson et al., 2014; Vatanen et al., 2016; Dedrick et al., 2020).

4.2 Dietary factors

We also compare the microbiome composition of groups of samples differentiated by each of the eight dietary factors introduced in Section 4.1. In particular, the cessation of breastfeeding and the introduction of other types of food are registered continuously. Thus we are essentially comparing the microbiome compositions in samples taken before and after those change points of diet. Similar to Section 4.1, we include the T1D status, other dietary covariates, and environmental covariates including age, gender and nationality as fixed effects, individuals as random effects in our mixed effects model. The sample size under different comparisons as well as the PJAPs with $\lambda = 10$ are shown in Table 2. Results with different values of λ are shown in Table S5 in the Online Supplementary Materials.

We visualize the cross-group differences by marking the PMAPs along the phylogenetic tree (Figure 8). For comparisons that reflect significant cross-group differences in microbiome compositions, the differences tend to occur at multiple nodes jointly and different dietary factors are associated with different sets of taxa. As opposed to seroconversion, the association between dietary variables with *Bacteroides* or *Erysipelotrichaceae* is weak; instead, many of the nodes with large PMAPs belong to the order *Clostridiales* (node A2 in Fig. 8). As shown in Fig. 9, this taxon has fairly consistent developmental patterns across infants.

Table 2: PJAPs of the dietary variables

Variable	Group size		PJAP
	On	Off	
Barley	531	246	1.00
Breastfeeding	248	529	1.00
Buckwheat and millet	198	579	0.98
Eggs	477	300	1.00
Fish	581	196	0.81
Rye	514	263	0.58
Solid food	681	96	1.00
Soy product	107	670	0.67

The relative abundance of Clostridiales is mostly close to 0 during early infancy. After the introduction of solid food, the relative abundance of Clostridiales increases until around 250 days after birth, then it stabilizes at around 0.5.

In addition to this common pattern, we investigate how breastfeeding shapes the gut microbiome development. In most infants in this study, the cessation of breastfeeding happened after introduction of solid food. In the comparison between samples collected before and after cessation of breastfeeding, for each node A with $\text{PMAP} > 0.5$, the taxa associated with the left and right child of this node, the common taxon they belong to, as well as $\hat{\alpha}(A)$, are summarized in Table 3. Positive $\hat{\alpha}(A)$ indicates higher abundance of taxa in the left child of A relative to those in the right child in the gut microbiome of infants who are still breastfed. The negative $\hat{\alpha}(A)$ at node 5 (Clostridiales) indicates higher abundance of the family Lachnospiraceae relative to other under the order Clostridiales in samples collected from infants after cessation of breastfeeding. Similar results of enrichment of Lachnospiraceae with cessation of breastfeeding have been reported in previous analysis of this dataset (Kostic et al., 2015) as well as other study on association between breastmilk and infant gut microbiota (Fehr et al., 2020). The positive $\hat{\alpha}(A)$ at node 34 indicates higher relative abundance of *Bifidobacterium bifidum* and *Bifidobacterium longum* in samples collected from infants during breastfeeding. This result is consistent to previous findings on the high abundance of *Bifidobacterium longum* in breastmilk and enrichment of *Bifidobacterium bifidum* in breastfed infants (Gueimonde et al., 2007; Fehr et al., 2020). Similar tables of the other grouping variables are shown in the Online Supplementary Materials (Table S6 - S10).

5 Conclusions

We have introduced the LTN model as a general-purpose model for microbiome compositions. LTN decomposes the multinomial sampling model to a collection of binomials at the interior nodes of the phylogenetic tree, and transforms OTU compositions to node-specific log-odds and adopts multivariate normal model on the log-odds, hence possesses the benefits of both LN and DT models. In particular, the multivariate normal model on the log-odds offers flexible covariance structure among OTUs. With the tree-based decomposition, LTN avoids the computational challenges caused by the lack of conjugacy between multinomial

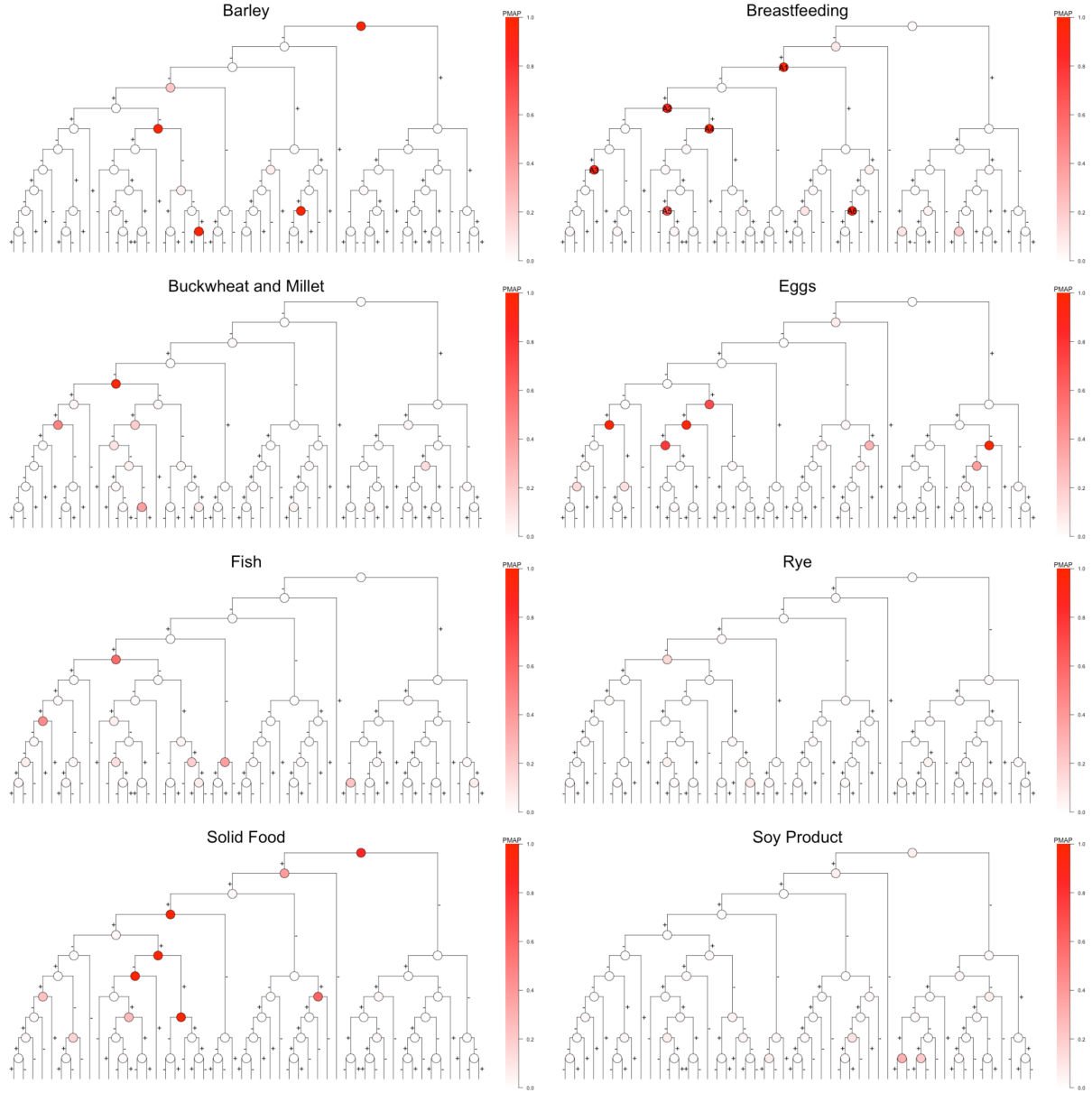


Figure 8: PMAP of the dietary variables. The nodes are colored by PMAP. For each node A , the sign of posterior mean of $\alpha(A)$ is marked with “+”/“-” on left and right branches.

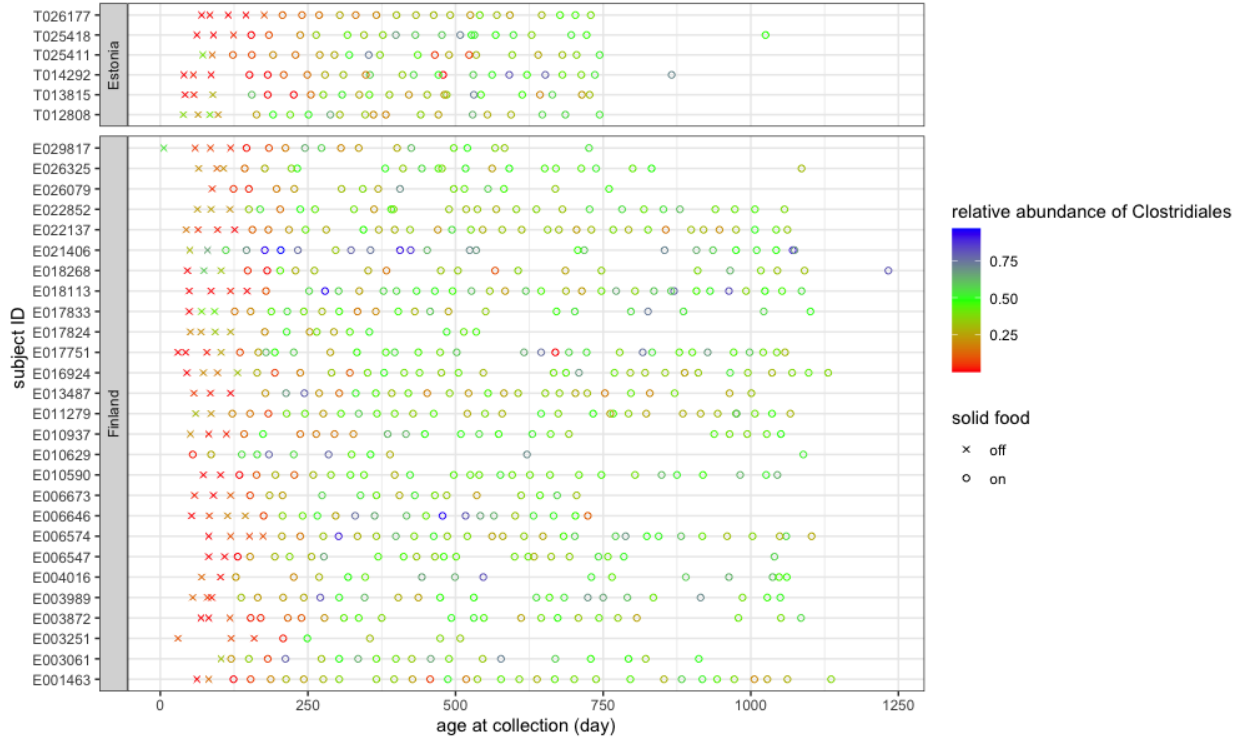


Figure 9: Relative abundance of Clostridiales

Table 3: Nodes with PMAP > 0.5 for breastfeeding

node	taxon in common	taxa on the left	taxa on the right	$\hat{\alpha}(A)$
A1	Bacteria	Firmicutes	Proteobacteria, Actinobacteria	-0.83
A2	Clostridiales	Lachnospiraceae	Ruminococcaceae, Clostridiaceae, Veillonellaceae	-0.84
A3	Lachnospiraceae	OTU 289734, OTU 4469576, OTU 3134492, OTU 197004	OTU 2724175	-1.30
A4	Clostridiales	Ruminococcaceae, Clostridiaceae	Veillonellaceae	-2.04
A5	Ruminococcus	OTU 146554	OTU 191153, OTU 265871	-1.45
A6	Bifidobacterium	longum, bifidum	adolescentis	1.43

and multivariate normal in LN models, and efficient inference can be carried out with Gibbs sampling by introducing Pólya-Gamma auxiliary variables. This opens the door to adopting a wide range of multivariate analysis models/methods for microbiome analysis while maintaining computational tractability.

The LTN model can be used either as a standalone model or a component in more sophisticated models involving microbiome compositions. We have provided two examples—namely, inference on the correlation structure and mixed-effects modeling—to demonstrate its broad applicability. In the covariance estimation example, we have adopted the graphical Lasso prior on the inverse covariance matrix of the log-odds to infer an underlying sparse graph among the interior nodes of the phylogenetic tree. In mixed-effects modeling, we have shown how to carry out cross-group comparison of microbiome compositions through a Bayesian model choice framework. In these examples, our model/prior choices can be substituted with other existing approaches as the practitioner sees fit in the given context.

Finally, we note that while our domain context is microbiome analysis, the LTN model is more broadly applicable to other compositional data along with a binary tree partition over the compositional categories. In other contexts, such a tree can often be obtained based on domain knowledge or from data-driven approaches such as hierarchical clustering. Beyond compositional data, tree-based log-odds decompositions can also be used as device for modeling general probability distributions (Jara and Hanson, 2011), the modeling and inference strategies can be generalized to such broader contexts as well.

Software

We provide an R package (LTN: <https://github.com/MaStatLab/LTN>) implementing the proposed method in this paper. Source code for the numerical examples and case study is available at https://github.com/MaStatLab/LTN_analysis.

Acknowledgment

This research is supported by NIH grant R01-GM135440.

References

- Äijö, T., C. L. Müller, and R. Bonneau (2017, 09). Temporal probabilistic modeling of bacterial compositions derived from 16S rRNA sequencing. *Bioinformatics* 34(3), 372–380.
- Aitchison, J. (1982). The statistical analysis of compositional data. *Journal of the Royal Statistical Society. Series B (Methodological)* 44(2), 139–177.
- Beghini, F., L. J. McIver, A. Blanco-Míguez, L. Dubois, F. Asnicar, S. Maharjan, A. Mailyan, P. Manghi, M. Scholz, A. M. Thomas, M. Valles-Colomer, G. Weingart, Y. Zhang, M. Zolfo, C. Huttenhower, E. A. Franzosa, and N. Segata (2021, May). Integrating taxonomic, functional, and strain-level profiling of diverse microbial communities with biobakery 3. *Elife* 10.

- Brugman, S., F. A. Klatter, J. T. J. Visser, A. C. M. Wildeboer-Veloo, H. J. M. Harmsen, J. Rozing, and N. A. Bos (2006). Antibiotic treatment partially protects against type 1 diabetes in the bio-breeding diabetes-prone rat. is the gut flora involved in the development of type 1 diabetes? *Diabetologia* 49(9), 2105–2108.
- Callahan, B. J., P. J. McMurdie, M. J. Rosen, A. W. Han, A. J. A. Johnson, and S. P. Holmes (2016). Dada2: High-resolution sample inference from illumina amplicon data. *Nature Methods* 13(7), 581–583.
- Cao, Y., W. Lin, and H. Li (2019). Large covariance estimation for compositional data via composition-adjusted thresholding. *Journal of the American Statistical Association* 114(526), 759–772.
- Davis-Richardson, A. G., A. N. Ardisson, R. Dias, V. Simell, M. T. Leonard, K. M. Kempainen, J. C. Drew, D. Schatz, M. A. Atkinson, B. Kolaczowski, J. Ilonen, M. Knip, J. Toppari, N. Nurminen, H. Hyöty, R. Veijola, T. Simell, J. Mykkänen, O. Simell, and E. W. Triplett (2014). Bacteroides dorei dominates gut microbiome prior to autoimmunity in finnish children at high risk for type 1 diabetes. *Frontiers in Microbiology* 5, 678.
- Dedrick, S., B. Sundaresh, Q. Huang, C. Brady, T. Yoo, C. Cronin, C. Rudnicki, M. Flood, B. Momeni, J. Ludvigsson, and E. Altindis (2020, 02). The role of gut microbiota and environmental factors in type 1 diabetes pathogenesis. *Frontiers in endocrinology* 11, 78–78.
- Dennis III, S. Y. (1991). On the hyper-dirichlet type 1 and hyper-liouville distributions. *Communications in Statistics - Theory and Methods* 20(12), 4069–4081.
- Egozcue, J. J. and V. Pawlowsky-Glahn (2016, July). Changing the Reference Measure in the Simplex and its Weighting Effects. *Austrian Journal of Statistics* 45(4), 25–44.
- Egozcue, J. J., V. Pawlowsky-Glahn, G. Mateu-Figueras, and C. Barceló-Vidal (2003, April). Isometric Logratio Transformations for Compositional Data Analysis. *Mathematical Geology* 35(3), 279–300.
- Fehr, K., S. Moossavi, H. Sbihi, R. C. T. Boutin, L. Bode, B. Robertson, C. Yonemitsu, C. J. Field, A. B. Becker, P. J. Mandhane, M. R. Sears, E. Khafipour, T. J. Moraes, P. Subbarao, B. B. Finlay, S. E. Turvey, and M. B. Azad (2020, Aug). Breastmilk feeding practices are associated with the co-occurrence of bacteria in mothers’ milk and the infant gut: the child cohort study. *Cell Host Microbe* 28(2), 285–297.
- Giongo, A., K. A. Gano, D. B. Crabb, N. Mukherjee, L. L. Novelo, G. Casella, J. C. Drew, J. Ilonen, M. Knip, H. Hyöty, R. Veijola, T. Simell, O. Simell, J. Neu, C. H. Wasserfall, D. Schatz, M. A. Atkinson, and E. W. Triplett (2011). Toward defining the autoimmune microbiome for type 1 diabetes. *The ISME Journal* 5(1), 82–91.
- Grantham, N., B. Reich, E. Borer, and K. Gross (2017, 03). Mimix: a bayesian mixed-effects model for microbiome data from designed experiments. *Journal of the American Statistical Association*.
- Gueimonde, M., K. Laitinen, S. Salminen, and E. Isolauri (2007). Breast milk: a source of bifidobacteria for infant gut development and maturation? *Neonatology* 92(1), 64–66.
- Jara, A. and T. E. Hanson (2011, 09). A class of mixtures of dependent tail-free processes. *Biometrika* 98(3), 553–566.
- Kostic, A. D., D. Gevers, H. Siljander, T. Vatanen, T. Hyötyläinen, A.-M. Hämäläinen, A. Peet, V. Tillmann, P. Pöhö, I. Mattila, H. Lähdesmäki, E. A. Franzosa, O. Vaarala, M. de Goffau, H. Harmsen, J. Ilonen, S. M. Virtanen, C. B. Clish, M. Orešič, C. Hutten-

- hower, M. Knip, and R. J. Xavier (2015, 2020/12/18). The dynamics of the human infant gut microbiome in development and in progression toward type 1 diabetes. *Cell Host & Microbe* 17(2), 260–273.
- La Rosa, P. S., J. P. Brooks, E. Deych, E. L. Boone, D. J. Edwards, Q. Wang, E. Sodergren, G. Weinstock, and W. D. Shannon (2012). Hypothesis testing and power calculations for taxonomic-based human microbiome data. *PloS one* 7(12), e52078–e52078.
- Mao, J., Y. Chen, and L. Ma (2020). Bayesian graphical compositional regression for microbiome data. *Journal of the American Statistical Association* 115(530), 610–624.
- McArdle, B. H. and M. J. Anderson (2001). Fitting multivariate models to community data: a comment on distance-based redundancy analysis. *Ecology* 82(1), 290–297.
- Polson, N. G., J. G. Scott, and J. Windle (2013). Bayesian inference for logistic models using pólya-gamma latent variables. *Journal of the American Statistical Association* 108(504), 1339–1349.
- Ren, B., S. Bacallado, S. Favaro, T. Vatanen, C. Huttenhower, and L. Trippa (2020, 03). Bayesian mixed effects models for zero-inflated compositions in microbiome data analysis. *Ann. Appl. Stat.* 14(1), 494–517.
- Silverman, J., A. Washburne, S. Mukherjee, and L. David (2017, February). A phylogenetic transform enhances analysis of compositional microbiota data. *eLife* 6.
- Silverman, J. D., H. K. Durand, R. J. Bloom, S. Mukherjee, and L. A. David (2018). Dynamic linear models guide design and analysis of microbiota studies within artificial human guts. *Microbiome* 6(1), 202.
- Tang, Y., L. Ma, and D. L. Nicolae (2018). A phylogenetic scan test on a Dirichlet-tree multinomial model for microbiome data. *The Annals of Applied Statistics* 12(1), 1 – 26.
- Vatanen, T., A. D. Kostic, E. d’Hennezel, H. Siljander, E. A. Franzosa, M. Yassour, R. Kolde, H. Vlamakis, T. D. Arthur, A.-M. Hämäläinen, A. Peet, V. Tillmann, R. Uibo, S. Mokuřov, N. Dorshakova, J. Ilonen, S. M. Virtanen, S. J. Szabo, J. A. Porter, H. Lähdesmäki, C. Huttenhower, D. Gevers, T. W. Cullen, M. Knip, D. S. Group, and R. J. Xavier (2016, 05). Variation in microbiome lps immunogenicity contributes to autoimmunity in humans. *Cell* 165(4), 842–853.
- Wang, H. (2012, 12). Bayesian graphical lasso models and efficient posterior computation. *Bayesian Anal.* 7(4), 867–886.
- Xia, F., J. Chen, W. K. Fung, and H. Li (2013, December). A Logistic Normal Multinomial Regression Model for Microbiome Compositional Data Analysis: Logistic Normal Multinomial Regression. *Biometrics* 69(4), 1053–1063.

Supplementary materials

A Gibbs sampler for the mixed-effects model in section 2.2.2

For notational simplicity, we rewrite the model in the following form:

$$\underset{n \times d}{\Psi} = \underset{n \times 11 \times d}{\mathbf{s}} \underset{n \times q_q \times d}{\alpha} + \underset{n \times q_q \times d}{\mathbf{Z}} \underset{n \times GG \times d}{\beta} + \underset{n \times GG \times d}{\mathbf{H}} \underset{n \times d}{\Gamma} + \underset{n \times d}{\epsilon},$$

where $H_{ij} = I(g_i = j)$. We denote the Pólya-Gamma auxiliary variable of node A and sample i with $w_i(A)$, and let $\Sigma_\epsilon = \text{diag}(\sigma_\epsilon^2(A) : A \in \mathcal{I})$, $\phi_\epsilon(A) = \sigma_\epsilon^{-2}(A) \sim \text{Gamma}(c_0, d_0)$.

The sampler cycles through the following steps:

- Sample β from

$$\beta|- \sim N_{q \times d}((\mathbf{Z}^T \mathbf{Z})^{-1} \mathbf{Z}^T (\Psi - \mathbf{H} \Gamma - \mathbf{s} \alpha) (\Sigma_\epsilon^{-1} + \mathbf{I}/(100n))^{-1} \Sigma_\epsilon^{-1}, \\ (\Sigma_\epsilon^{-1} + \mathbf{I}/(100n))^{-1} \otimes (\mathbf{Z}^T \mathbf{Z})^{-1}).$$

- For each $A \in \mathcal{I}$, sample $\alpha(A)$ from

$$\alpha(A)|- \sim (1 - \pi'(A)) \delta_0(\alpha(A)) + \pi'(A) (1 - \delta_0(\alpha(A))) N(b(A) s_\alpha^2(A), s_\alpha^2(A)),$$

where

$$\pi'(A) = \frac{\pi(A) s_\alpha(A) \phi_\alpha^{1/2} \exp\{b^2(A) s_\alpha^2(A)/2\}}{1 - \pi(A) + \pi(A) s_\alpha(A) \phi_\alpha^{1/2} \exp\{b^2(A) s_\alpha^2(A)/2\}}, \\ s_\alpha(A) = (\phi_\alpha + \sum_{i=1}^N s_i^2 \phi_\epsilon(A))^{-1/2}, b(A) = \phi_\epsilon(A) \sum_{i=1}^N (s_i(\psi_i(A) - \gamma_i(A) - \mathbf{z}_i^T \beta(A))).$$

- For each $A \in \mathcal{I}$, sample $\pi(A)$ from

$$\pi(A)|- \sim \text{Beta}(m + 1 - I(\alpha(A) = 0), 1 - m + I(\alpha(A) = 0)).$$

- For $l = 1, \dots, G$, let

$$n_l = \sum_{i=1}^n I(g_i = l), \mathbf{C}_l = (n_l \Sigma_\epsilon^{-1} + \mathbf{\Omega})^{-1}, \mathbf{m}_l = \mathbf{C}_l (\Sigma_\epsilon^{-1} \sum_{i: g_i=l} (\psi_i - \beta^T \mathbf{z}_i - s_i \alpha^T)),$$

and sample γ_l from

$$\gamma_l|- \sim N(\mathbf{m}_l, \mathbf{C}_l).$$

- For each $A \in \mathcal{I}$, sample $\phi_\epsilon(A)$ from

$$\phi_\epsilon(A)|- \sim \text{Gamma}(c_0 + n/2, d_0 + \sum_{i=1}^n \epsilon_i^2(A)/2)$$

- For $i = 1, \dots, n$, let

$$\mathbf{C}_i = (\text{diag}(\mathbf{w}_i) + \Sigma_\epsilon^{-1})^{-1}, \mathbf{m}_i = \mathbf{C}_i(\boldsymbol{\kappa}_i + \Sigma_\epsilon^{-1}(\boldsymbol{\beta}^T \mathbf{z}_i + \boldsymbol{\gamma}_{g_i} + s_i \boldsymbol{\alpha}^T)),$$

then sample $\boldsymbol{\psi}_i$ from

$$\boldsymbol{\psi}_i | - \sim N(\mathbf{m}_i, \mathbf{C}_i)$$

- For $i = 1, \dots, n$ and for each $A \in \mathcal{I}$, sample the Pólya-Gamma variable $w_i(A)$ from

$$w_i(A) | - \sim \text{PG}(y_i(A), \psi_i(A))$$

- Sample ϕ_α from

$$\phi_\alpha | - \sim \text{Gamma}(t + \sum_{A \in \mathcal{I}} I(\alpha(A) \neq 0)/2, u + \sum_{A \in \mathcal{I}} \alpha^2(A)/2)$$

- Update $\boldsymbol{\Omega}$ with the block Gibbs sampling procedure described in section 2.2.1, where the data-augmented target distribution is given by Eq.(4) and $\mathbf{S} = \boldsymbol{\Gamma}^T \boldsymbol{\Gamma}$.

B Additional tables and figures

Table S1: Risks of LTN with different λ under LN-hub scenario

	$\lambda = 0.1$	$\lambda = 1$	$\lambda \sim \text{Ga}(1, 0.01)$
Frobenius	20.04	20.68	19.00
L_1	30.21	29.04	27.95
L_∞	1.39	1.39	1.24
Spectral	17.21	18.43	16.97

Table S2: Risks of LTN with different λ under LN-block scenario

	$\lambda = 0.1$	$\lambda = 1$	$\lambda \sim \text{Ga}(1, 0.01)$
Frobenius	19.30	19.67	17.58
L_1	28.96	27.41	26.42
L_∞	1.38	1.39	1.24
Spectral	16.38	17.31	15.35

We label the internal nodes of the phylogenetic tree as shown in Fig. S1. The nodes with $\text{PMAP} > 0.5$ for the dietary variables are shown in Table S6 - S10.

Table S3: Risks of LTN with different λ under LN-sparse scenario

	$\lambda = 0.1$	$\lambda = 1$	$\lambda \sim \text{Ga}(1, 0.01)$
Frobenius	20.39	20.92	20.62
L_1	31.04	31.10	31.43
L_∞	1.39	1.40	1.35
Spectral	17.09	17.98	16.93

Table S4: Risks of LTN with different λ under DTM scenario

	$\lambda = 0.1$	$\lambda = 1$	$\lambda \sim \text{Ga}(1, 0.01)$
Frobenius	6.26	5.57	4.67
L_1	6.93	6.33	5.90
L_∞	0.79	0.72	0.62
Spectral	3.20	3.17	3.06

Table S5: PJAPs of grouping variables under different λ in DIABIMMUNE data analysis

Grouping variable	$\lambda = 1$	$\lambda = \sqrt{10}$	$\lambda = 10$
Barley	1.00	1.00	1.00
Breastfeeding	1.00	1.00	1.00
Buckwheat and Millet	0.53	0.60	0.99
Case/Control	0.51	0.51	0.49
Eggs	1.00	1.00	1.00
Fish	1.00	1.00	0.81
Rye	0.62	0.52	0.58
Seroconversion	1.00	1.00	1.00
Solid Food	1.00	1.00	1.00
Soy Product	0.88	0.91	0.67

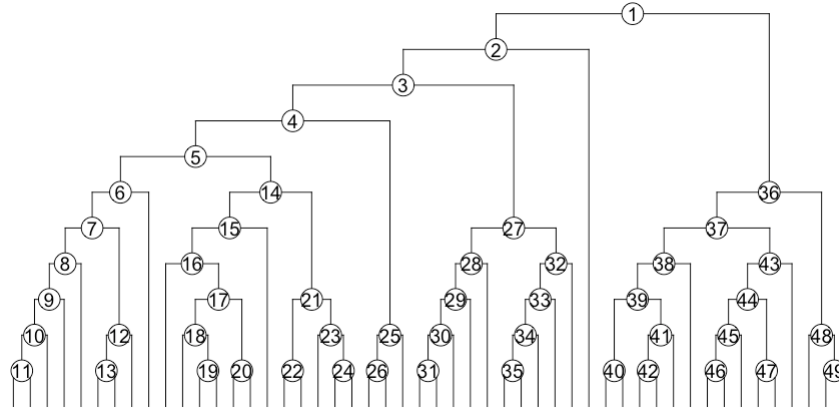


Figure S1: Labels for the internal nodes

Table S6: Nodes with PMAP > 0.5 for solid food

node	taxon in common	taxa on the left	taxa on the right	$\hat{\alpha}(A)$
1	Bacteria	Firmicutes, Proteobacteria, Actinobacteria, Verrucomicrobia	Bacteroidetes	0.86
4	Firmicutes	Clostridia	Erysipelotrichi, Bacilli	1.6
14	Clostridiales	Ruminococcaceae, Clostridiaceae	Veillonellaceae	-2.23
15	Clostridiales	Ruminococcaceae	Clostridiaceae	-4.38
21	Veillonellaceae	Dialister, Megaspheera	Veillonella	-3.59
32	Actinobacteria	Actinobacteria	Coriobacteriia	1.3

Table S7: Nodes with PMAP > 0.5 for eggs

node	taxon in common	taxa on the left	taxa on the right	$\hat{\alpha}(A)$
7	Lachnospiraceae	289734, 4469576, 3134492, 197004, 2724175	3926480, 177515, 182289	-1.42
14	Clostridiales	Ruminococcaceae, Clostridiaceae	Veillonellaceae	0.96
15	Clostridiales	Ruminococcaceae	Clostridiaceae	2.18
16	Ruminococcaceae	Oscillospira	Ruminococcus, unclassified, Faecalibacterium	-1.3
43	Bacteroides	ovatus, caccae, uniformis	fragilis	-1.79

Table S8: Nodes with PMAP > 0.5 for fish

node	taxon in common	taxa on the left	taxa on the right	$\hat{\alpha}(A)$
5	Clostridiales	Lachnospiraceae	Ruminococcaceae, Clostridiaceae, Veillonellaceae	0.77

Table S9: Nodes with PMAP > 0.5 for barley

node	taxon in common	taxa on the left	taxa on the right	$\hat{\alpha}(A)$
1	Bacteria	Firmicutes, Proteobacteria, Actinobacteria, Verrucomicrobia	Bacteroidetes	-1.23
14	Clostridiales	Ruminococcaceae, Clostridiaceae	Veillonellaceae	2.03
24	dispar	4453501	4388775	2.08
34	Bifidobacterium	longum, bifidum	adolescentis	-1.44

Table S10: Nodes with PMAP > 0.5 for buckwheat and millet

node	taxon in common	taxa on the left	taxa on the right	$\hat{\alpha}(A)$
5	Clostridiales	Lachnospiraceae	Ruminococcaceae, Clostridiaceae, Veillonellaceae	1.26

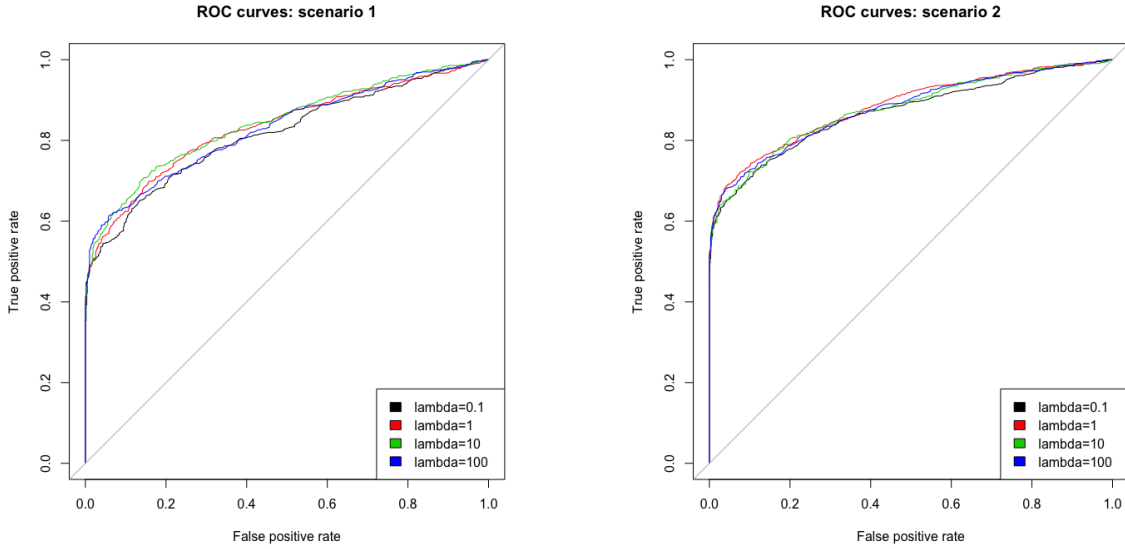


Figure S2: ROC curves of LTN in cross-group comparison examples